Supplementary Information File

Flexible KNN-BT-Poly(vinylidene fluoride) Composites: Synergistic Effect on Ferroelectric Properties and Capacitive Pressure Sensing Response

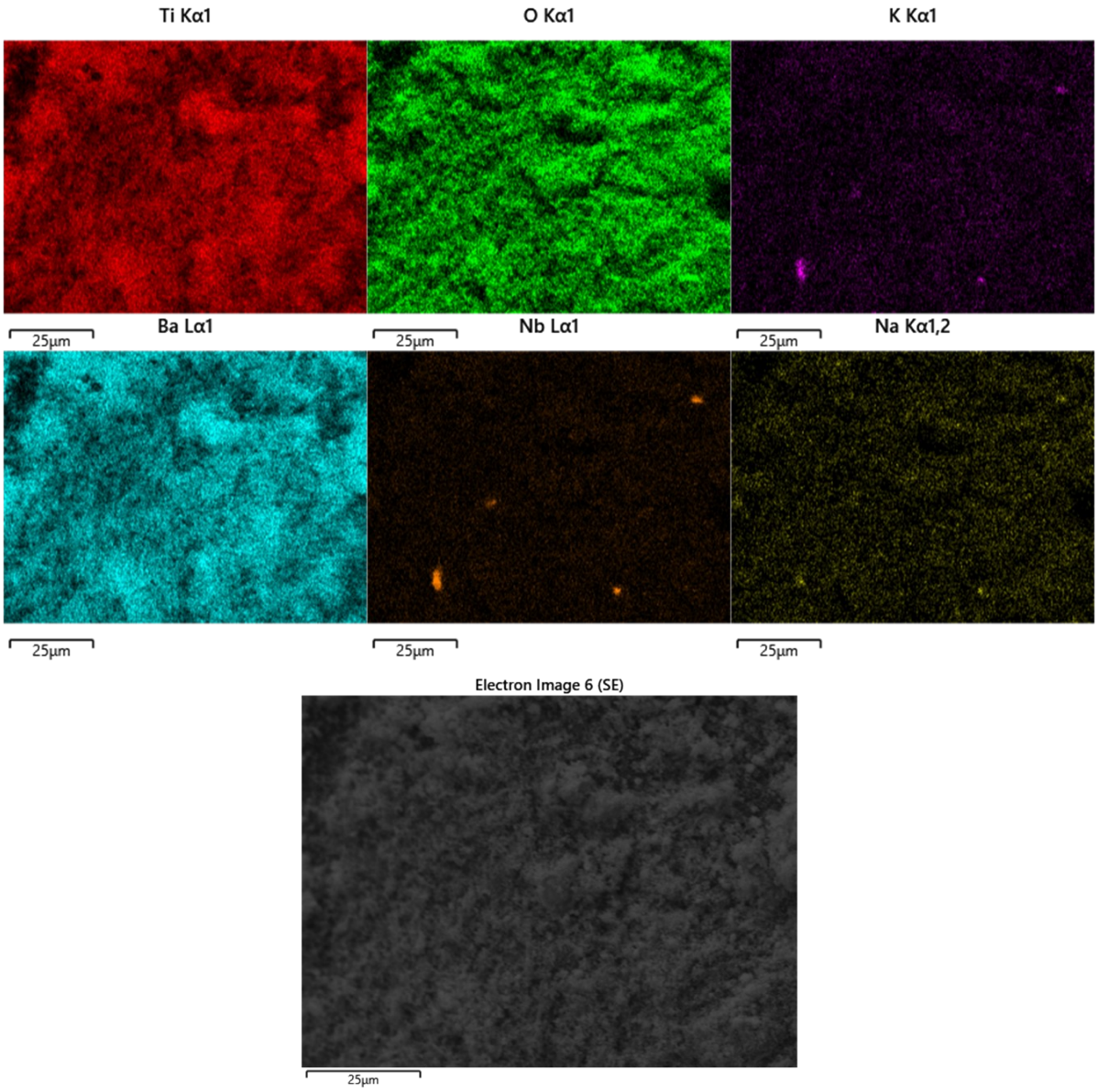

Figure S1 Elemental mapping of 1% KNN-BT ceramics using EDS

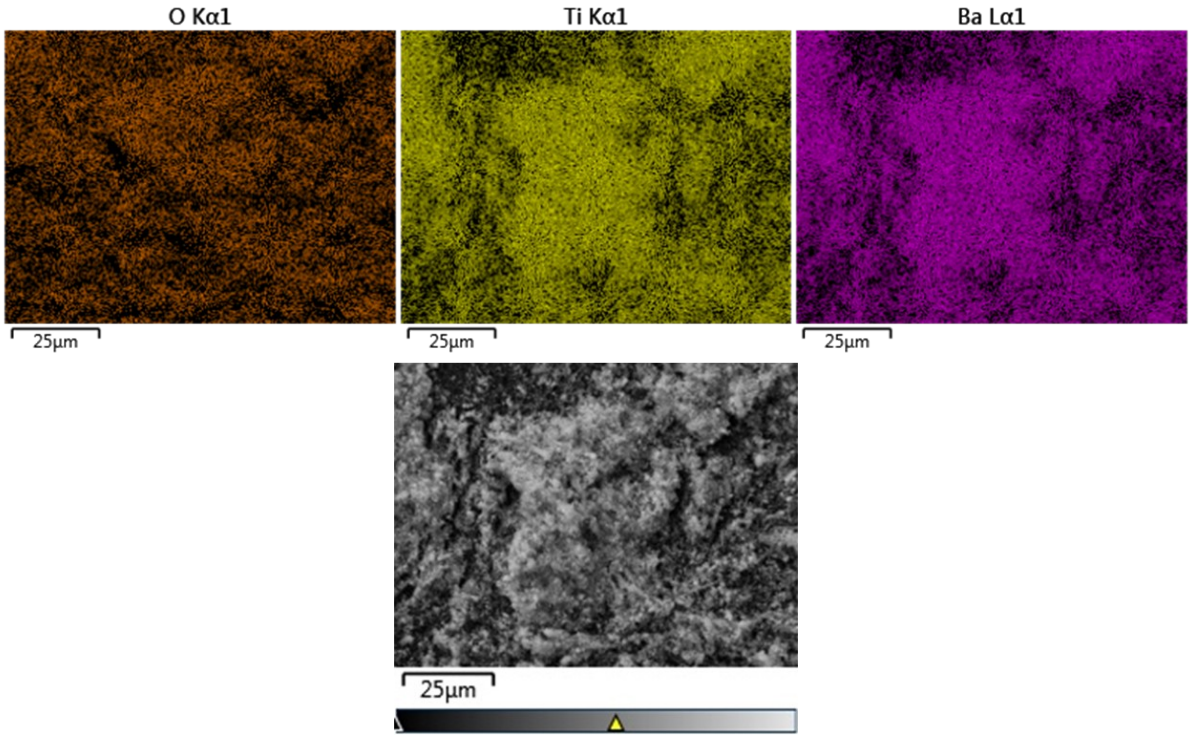

Figure S2 Elemental mapping of $BaTiO_3$ ceramics using EDS

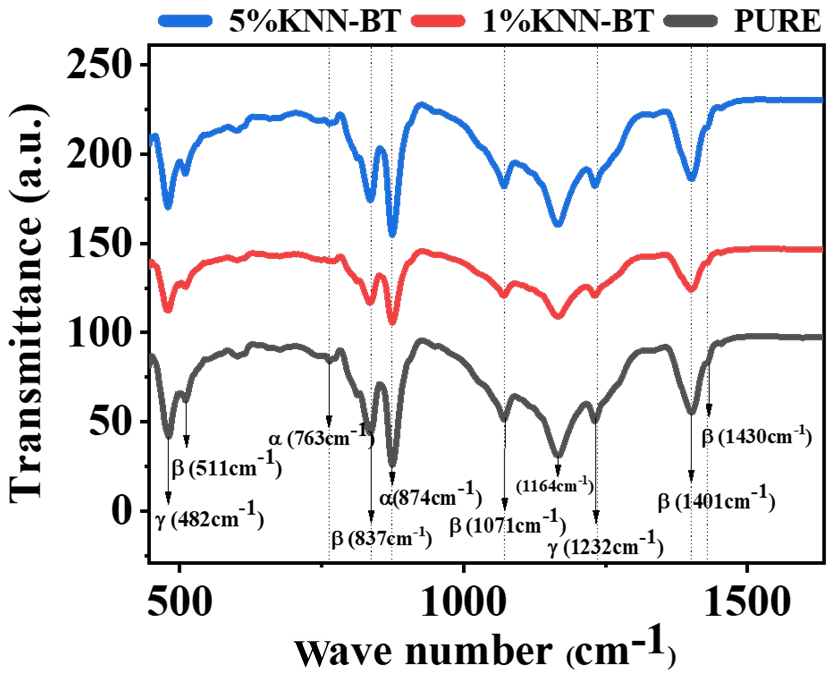

Figure S3 FT-IR analysis of pristine PVDF, 1% (1% KNN-BT)/PVDF composite, and 5% (1% KNN-BT)/PVDF

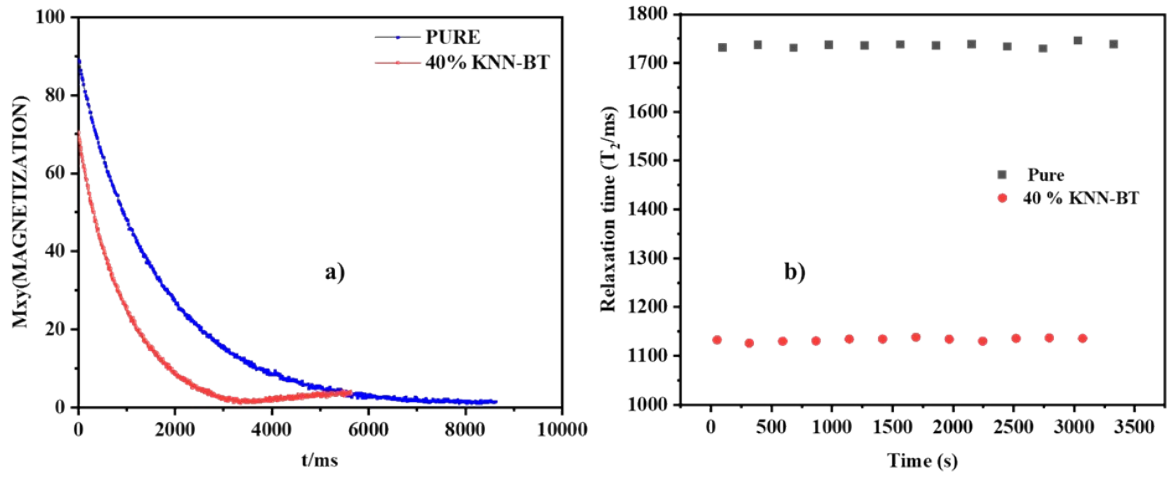

Figure S4 Stability analysis of the 40%(1%KNN)-BT/PVDF composite and pristine PVDF

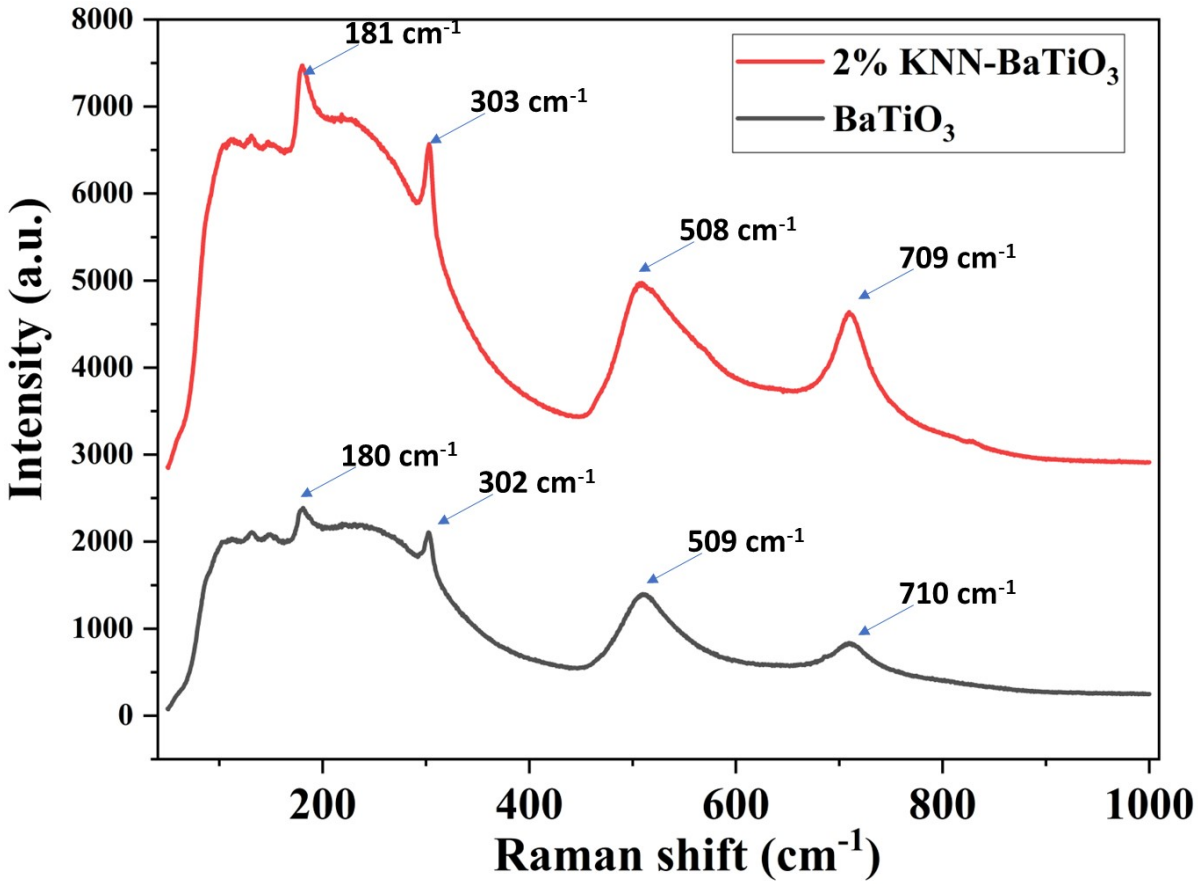

Figure S5 Raman spectra of pristine $BaTiO_3$ and 2 wt% KNN-$BaTiO_3$ samples

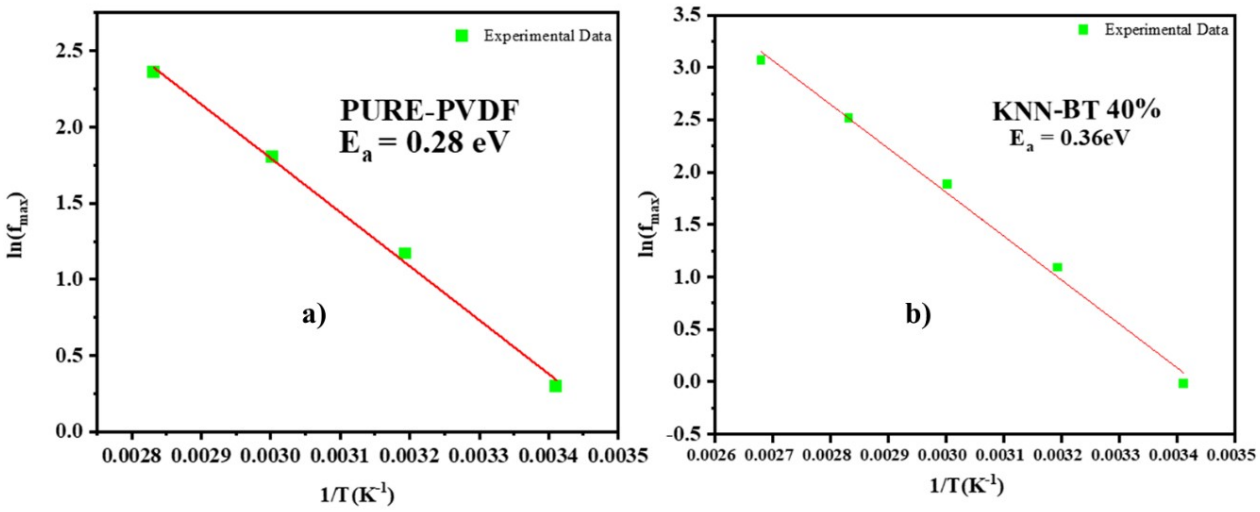

Figure S6 Activation energy plot of a) PVDF and b) 40% (1%KNN)-BT/PVDF composite

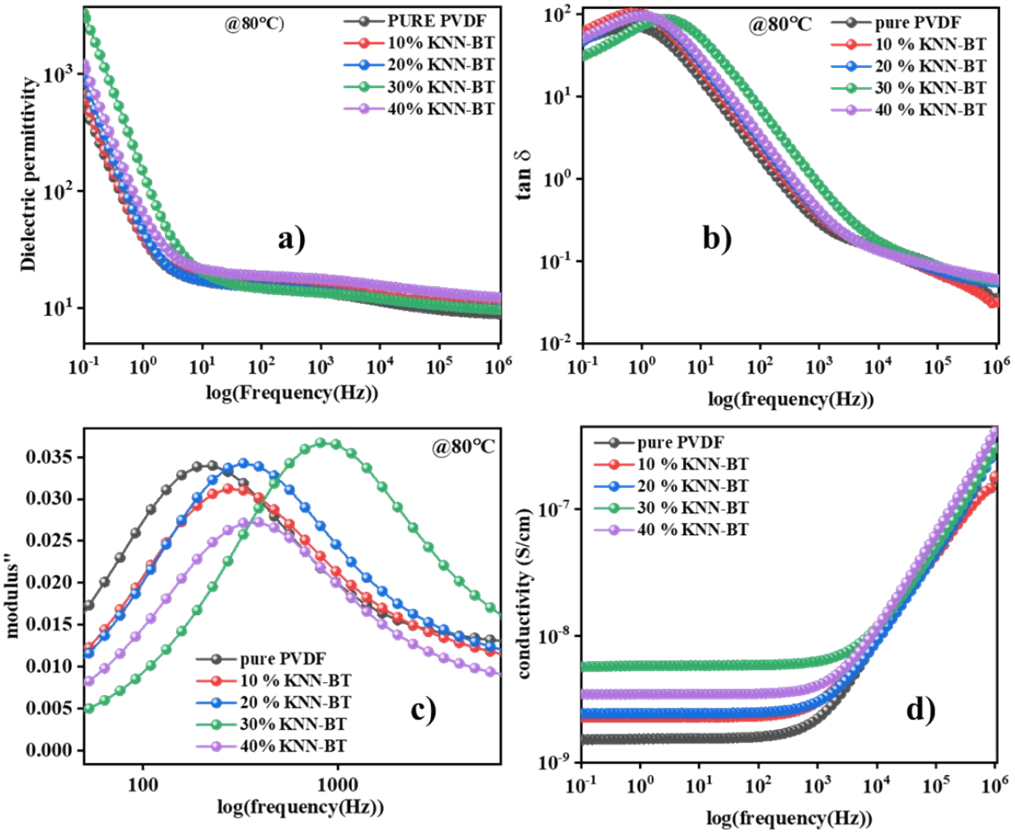

Figure S7 The dielectric properties comparison for all prepared flexible composites with pristine PVDF at 80 °C, a) dielectric permittivity, b) dielectric loss tangent, c) imaginary electric modulus, d) conductivity

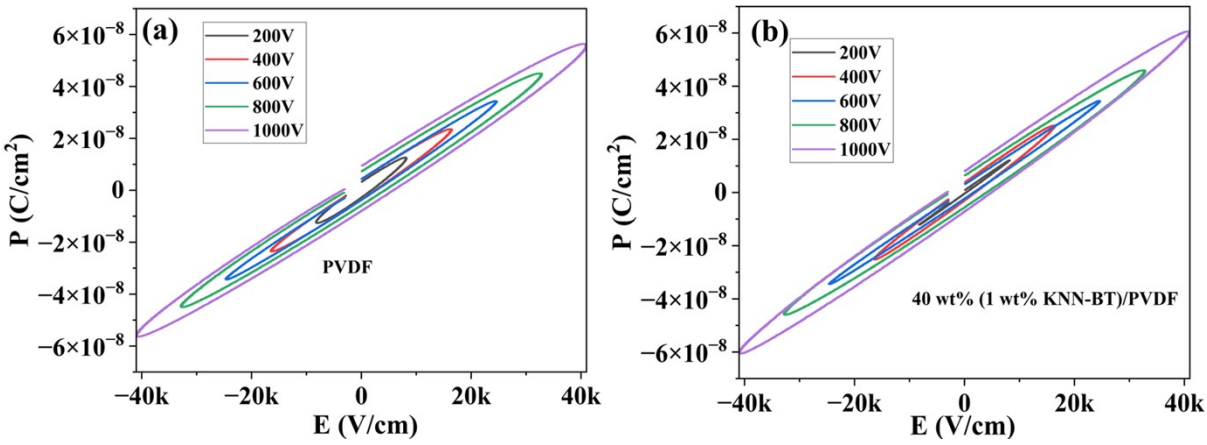

Figure S8 The P-E loop measurements for the (a) pure PVDF film, and (b) 40 wt% (1 wt% KNN-BT/PVDF) composite film as a function of applied voltage

Note: The dimensions of the prepared sensing devices and samples for dielectric measurements are: circular discs of 20 mm, with electroding on both sides, with conducting tape

Table S1: The dielectric properties of KNN-$BaTiO_3$ composite ceramics measured at room temperature and ~1 Hz

Sr. No.	**Sample**	ϵ'	σ **(S/cm)**	**Tan**δ
1	$BaTiO_3$	202.6	8.9×10^{-11}	0.79
2	0.5 wt% KNN-$BaTiO_3$	196.8	4.0×10^{-11}	0.36
3	1 wt% KNN-$BaTiO_3$	264.0	10.6×10^{-11}	0.72
4	2 wt% KNN-$BaTiO_3$	199.4	4.93×10^{-11}	0.44

Table S2: The dielectric properties of (1% KNN-$BaTiO_3$)/PVDF flexible composites measured at room temperature and ~1 Hz

Sr. No.	**Sample**	ϵ'	σ **(S/cm)**	**Tan**δ
1	PVDF	15.1	1.33×10^{-11}	1.58
2	10% (1% KNN-$BaTiO_3$)/PVDF	17.1	1.87×10^{-11}	1.96
3	20% (1% KNN-$BaTiO_3$)/PVDF	18.5	1.91×10^{-11}	1.86
4	30% (1% KNN-$BaTiO_3$)/PVDF	20.6	4.83×10^{-11}	4.21
5	40% (1% KNN-$BaTiO_3$)/PVDF	21.36	0.78×10^{-11}	0.66
6	50% (1% KNN-$BaTiO_3$)/PVDF	20.9	1.9×10^{-11}	1.63

Table S3: The dielectric properties of (1% KNN-$BaTiO_3$)/PVDF flexible composites measured at room temperature and ~1 kHz

Sr. No.	**Sample**	ϵ'	σ **(nS/cm)**	**Tan**δ	**Ref**
1	PVDF	9.56	0.57	0.09	This work
2	10% (1% KNN-$BaTiO_3$)/PVDF	11.50	0.62	0.08	This work
3	20% (1% KNN-$BaTiO_3$)/PVDF	12.50	0.73	0.09	This work
4	30% (1% KNN-	14.24	0.97	0.10	This work

	$BaTiO_3$)/PVDF				
5	40% (1% KNN-$BaTiO_3$)/PVDF	15.20	0.87	0.09	This work
6	50% (1% KNN-$BaTiO_3$)/PVDF	15.00	1.00	0.10	This work

Table S4: The dielectric properties of PVDF-based flexible composites measured at room temperature and ~1 kHz from literature [1][2]

Sr. No.	**Sample**	ϵ	**Tanδ**	**Ref**
1	$BaTiO_3$/PVDF	24	0.02	[3]
2	$BaSnF_4$/PVDF	20.5	0.095	[4]
3	$Ba_{0.6}Sr_{0.4}TiO_3$/PVDF	20.56	0.02	[5]
4	$SrTiO_3$@SiO_2/PVDF-CTFE	12.8	0.025	[6]
5	$NaNbO_3$/PVDF	15.3	0.03	[7]
6	$Ba_{0.7}Sr_{0.3}TiO_3$/PVDF-HFP	14	0.04	[8]
7	PVDF/$BaTiO_3$/RGO	12	0.88	[9]
8	PVDF/$BaTiO_3$ hollow nanospheres	10	0.90	[10]
9	KNN-BT/PVDF	15.20	0.09	**This work**

Table S5: The capacitive pressure-sensing properties of the composites measured at room temperature from the literature

Sr. No.	Sample	Sensitivity	Ref
1	PDMS-PEDOT:PSS/MXene-PVDF-TrFF	0.51 kPa^{-1}	[11]
2	Polyurethane-PVDF	0.3 kPa^{-1}	[12]
3	KNN-BT/PVDF	0.297 kPa^{-1}	**This work**
4	micropillar–PVDF	0.430 kPa-1	[13]
5	(PVDF-TrFE) fiber-TiO_2 pillar TiO_2	0.163 kPa^{-1}	[14]
6	Nanpillars-PVDF-TrFE	0.35 kPa^{-1}	[15]

Table S6: The approximate average thickness of the prepared composite films

Sr. No.	Sample	Thickness (std. dev.: 0.01 mm)
1	PVDF	0.16 mm
2	10% (1% KNN-$BaTiO_3$)/PVDF	0.20 mm
3	20% (1% KNN-$BaTiO_3$)/PVDF	0.20 mm
4	30% (1% KNN-$BaTiO_3$)/PVDF	0.21 mm
5	40% (1% KNN-$BaTiO_3$)/PVDF	0.22 mm
6	50% (1% KNN-$BaTiO_3$)/PVDF	0.19 mm

References

[1] J. Zhou, D. Hou, S. Cheng, J. Zhang, W. Chen, L. Zhou, P. Zhang, Recent advances in dispersion and alignment of fillers in PVDF-based composites for high-performance

dielectric energy storage, Mater. Today Energy. 31 (2023) 101208. https://doi.org/10.1016/j.mtener.2022.101208.

[2] E.C. Silva, J.P. da Silva, F.X. Nobre, L. Aguilera, M.R. Morelli, A.P. Luz, Y. Leyet, Flexible PVDF/$BaTiO_3$ composites for electromechanical applications: Effect of $BaTiO_3$ content and phase evolution, J. Alloys Compd. 1051 (2026) 185954. https://doi.org/10.1016/j.jallcom.2026.185954.

[3] T. Zhou, J.-W. Zha, R.-Y. Cui, B.-H. Fan, J.-K. Yuan, Z.-M. Dang, Improving Dielectric Properties of $BaTiO_3$ /Ferroelectric Polymer Composites by Employing Surface Hydroxylated $BaTiO_3$ Nanoparticles, ACS Appl. Mater. Interfaces. 3 (2011) 2184–2188. https://doi.org/10.1021/am200492q.

[4] C.-Y. Cho, S.-H. Kim, J.-W. Ha, H.S. Kang, E.-H. Sohn, I.J. Park, G.-R. Yi, S.G. Lee, High Dielectric Constant and Low Percolation Threshold in Poly(vinylidene fluoride) Composite Films Containing Mechanochemically Synthesized BaSnF 4 Nanowires, ACS Appl. Electron. Mater. 1 (2019) 2355–2362. https://doi.org/10.1021/acsaelm.9b00537.

[5] Z.B. Pan, L.M. Yao, J.W. Zhai, S.H. Liu, K. Yang, H.T. Wang, J.H. Liu, Fast discharge and high energy density of nanocomposite capacitors using Ba 0.6 Sr 0.4 TiO 3 nanofibers, Ceram. Int. 42 (2016) 14667–14674. https://doi.org/10.1016/j.ceramint.2016.06.090.

[6] B. Xie, L. Zhang, M.A. Marwat, Y. Zhu, W. Ma, P. Fan, H. Zhang, High energy storage performance for dielectric film capacitors by designing 1D SrTiO 3 @SiO 2 nanofillers, J. Adv. Dielectr. 08 (2018) 1850039. https://doi.org/10.1142/S2010135X1850039X.

[7] Z. Pan, L. Yao, G. Ge, B. Shen, J. Zhai, High-performance capacitors based on

NaNbO 3 nanowires/poly(vinylidene fluoride) nanocomposites, J. Mater. Chem. A. 6 (2018) 14614–14622. https://doi.org/10.1039/C8TA03084G.

[8] S. Wang, X. Huang, G. Wang, Y. Wang, J. He, P. Jiang, Increasing the Energy Efficiency and Breakdown Strength of High-Energy-Density Polymer Nanocomposites by Engineering the Ba 0.7 Sr 0.3 TiO 3 Nanowire Surface via Reversible Addition–Fragmentation Chain Transfer Polymerization, J. Phys. Chem. C. 119 (2015) 25307–25318. https://doi.org/10.1021/acs.jpcc.5b09066.

[9] N.D. Kulkarni, P. Kumari, Role of rGO on mechanical, thermal, and piezoelectric behaviour of PVDF-BTO nanocomposites for energy harvesting applications, J. Polym. Res. 30 (2023) 79. https://doi.org/10.1007/s10965-023-03449-4.

[10] S. Cho, J.S. Lee, J. Jang, Enhanced Crystallinity, Dielectric, and Energy Harvesting Performances of Surface-Treated Barium Titanate Hollow Nanospheres/PVDF Nanocomposites, Adv. Mater. Interfaces. 2 (2015). https://doi.org/10.1002/admi.201500098.

[11] S. Sharma, A. Chhetry, M. Sharifuzzaman, H. Yoon, J.Y. Park, Wearable Capacitive Pressure Sensor Based on MXene Composite Nanofibrous Scaffolds for Reliable Human Physiological Signal Acquisition, ACS Appl. Mater. Interfaces. 12 (2020) 22212–22224. https://doi.org/10.1021/acsami.0c05819.

[12] G. Kaur, J.S. Meena, M. Jassal, A.K. Agrawal, Hybrid Piezo-Capacitive Multimodal Sensors Based on Polyurethane–Poly(vinylidene fluoride) Nanofibers for Wearable E-Textiles, ACS Appl. Electron. Mater. 5 (2023) 3298–3308. https://doi.org/10.1021/acsaelm.3c00346.

[13] Z. Luo, J. Chen, Z. Zhu, L. Li, Y. Su, W. Tang, O.M. Omisore, L. Wang, H. Li, High-Resolution and High-Sensitivity Flexible Capacitive Pressure Sensors Enhanced by a

Transferable Electrode Array and a Micropillar–PVDF Film, ACS Appl. Mater. Interfaces. 13 (2021) 7635–7649. https://doi.org/10.1021/acsami.0c23042.

[14] H. Niu, H. Li, Y. Li, W. Yue, S. Gao, X. Wei, G. Shen, Cocklebur-inspired "branch-seed-spininess" 3D hierarchical structure bionic electronic skin for intelligent perception, Nano Energy. 107 (2023) 108144. https://doi.org/10.1016/j.nanoen.2022.108144.

[15] Y. Guo, S. Gao, W. Yue, C. Zhang, Y. Li, Anodized Aluminum Oxide-Assisted Low-Cost Flexible Capacitive Pressure Sensors Based on Double-Sided Nanopillars by a Facile Fabrication Method, ACS Appl. Mater. Interfaces. 11 (2019) 48594–48603. https://doi.org/10.1021/acsami.9b17966.